Fast Spatially Resolved Exhaust Gas Recirculation (EGR) Distribution Measurements in an Internal Combustion Engine Using Absorption Spectroscopy

Jihyung Yoo,[a] Vitaly Prikhodko,[a] James E. Parks,[a] Anthony Perfetto,[b] Sam Geckler,[b] William P. Partridge[a,*]

[a] *National Transportation Research Center, Fuels, Engines, and Emissions Research Center, Oak Ridge National Laboratory, 2360 Cherahala Boulevard, Knoxville, TN 37932 USA*

[b] *Cummins Inc.. Cummins Technical Center, 1900 McKinley Avenue, Columbus, IN 47201 USA*

Exhaust gas recirculation (EGR) in internal combustion engines is an effective method of reducing NO_x emissions while improving efficiency. However, insufficient mixing between fresh air and exhaust gas can lead to cycle-to-cycle and cylinder-to-cylinder non-uniform charge gas mixtures of a multi-cylinder engine, which can in turn reduce engine performance and efficiency. A sensor packaged into a compact probe was designed, built and applied to measure spatiotemporal EGR distributions in the intake manifold of an operating engine. The probe promotes the development of more efficient and higher-performance engines by resolving high-speed in situ CO_2 concentration at various locations in the intake manifold. The study employed mid-infrared light sources tuned to an absorption band of CO_2 near 4.3 μm, an industry standard species for determining EGR fraction. The calibrated probe was used to map spatial EGR distributions in an intake manifold with high accuracy and monitor cycle-resolved cylinder-specific EGR fluctuations at a rate of up to 1 kHz.

Index Headings: **Exhaust gas recirculation; EGR; Carbon dioxide; CO_2; Combustion; Uniformity; Light-emitting diode; LED.**

INTRODUCTION

Exhaust gas recirculation (EGR) is a principle technique to curb mono-nitrogen oxides (NO_x) emissions from internal combustion (IC) engines. It is widely used in both gasoline and diesel engines and mainly functions by reducing the peak combustion temperature. Exhaust gas recirculation is implemented by metering a portion of the exhaust into the intake flow via an EGR valve; the duct and valve required for this can be referred to as the EGR hardware, which uses a heat exchanger to cool the recirculated exhaust. For a given engine speed without EGR, NO_x generation rate is dictated by the fueling rate,[1] because thermal NO_x formation during combustion is highly temperature dependent.[2] Adding EGR to the intake charge gas mixture increases the specific heat capacity of the combustion mixture, thereby reducing peak combustion temperature. For diesel engines, it also reduces the molecular oxygen (O_2) concentration from the working fluid resulting in further reduction of NO_x.[3,4] Although a higher EGR fraction can lead up to a 25% reduction in NO_x emission,[5] it can also substantially increase ignition delay times, thereby introducing cycle-to-cycle variations.[5–7] These variations coupled with incomplete mixing of the EGR-air charge can induce dissimilar charge gas composition (fuel, air, and exhaust gas) between the combustion chambers of a multi-cylinder engine and lead to cylinder-to-cylinder variations.[8] Moreover, excessive EGR fraction in an internal EGR configuration can cause combustion phasing delays and lead to engine knock and misfire under certain conditions.[9] Overall, improper use of EGR can lead to unstable operation and reduce engine durability.[10]

Carbon dioxide (CO_2) is one of the major exhaust-gas constituents[11] and is of specific interest since it is commonly used to determine EGR fraction, defined as $([CO_{2,intake}] - [CO_{2,air}])/[CO_{2,exhaust}]$. The CO_2 concentration in ambient air ($[CO_{2,air}]$) is slowly varying and practically constant over typical engine-experiment timescales. Its variations can be monitored and accounted for with a separate slow (e.g., Fourier transfer infrared, FT-IR) measurement. The intake-charge-gas CO_2 concentration ($[CO_{2,intake}]$) is primarily due to EGR. For a well-controlled and optimized engine, exhaust CO_2 concentration ($[CO_{2,exhaust}]$) is temporally uniform indicating correspondingly uniform cylinder-to-cylinder and cycle-to-cycle combustion events. In the more likely case of imperfectly balanced combustion, individual cylinder-exhaust events will create temporally varying exhaust CO_2, which will in turn propagate through the EGR hardware to produce CO_2 (EGR) dynamics in the intake. In addition, exhaust-manifold pressure dynamics can exacerbate intake EGR dynamics due to temporally distinct and sequenced cylinder exhaust events, which can induce cylinder-to-cylinder and cycle-to-cycle combustion variations depending on their phasing versus the intake valve phasing, mixing, and other intake manifold design characteristics. The study of complex spatiotemporal EGR distributions in the intake manifold requires a diagnostic technique with sufficient temporal and spatial resolution. Moreover, a fast transient CO_2 measurement technique can be applied to rapidly assess combustion stability and uniformity for mitigating cylinder-to-cylinder and cycle-to-cycle combustion variations.

Absorption is a well-established spectroscopic diagnostic strategy for measuring flow-field parameters.[12,13] It is particularly useful in combustion diagnostics because absorption measurements are highly selective and very fast, up to 40 kHz using wavelength modulation spectroscopy with second-harmonic detection,[14] and can be applied to quantify parameters such as temperature

Received 18 November 2014; accepted 10 March 2015.

* Author to whom correspondence should be sent. E-mail: partridgewp@ornl.gov.

DOI: 10.1366/14-07796

0003-7028/15/6909-1047/0

and concentration without disturbing the flow of interest.[15,16] Absorption-based diagnostics are employed in a broad range of applications from fundamental studies of chemical-kinetic parameters in shock tubes[17] to commercial sensors for emission control.[18] Measurements have been demonstrated using a wide variety of sources ranging from vacuum ultraviolet (below 200 nm) to mid-infrared (MIR; up to 20 μm) sources. The MIR spectrum is of special interest for combustion applications since many combustion intermediate and product species have distinct absorption features in this region,[19] and advanced optical diagnostic techniques[20] can be utilized to enable high-sensitivity absorption detection. With the recent development of MIR light sources and detectors, novel diagnostic techniques based on MIR absorption are rapidly being developed for energy applications.

The sensor was designed as a lightweight cost-effective diagnostics technique dedicated to CO_2 measurements. The same concept could be applied to other broadband light sources such as a tungsten-halide lamp for measuring EGR in the intake[21] or simultaneously probing CO_2 and water (H_2O).[22] These studies are all based on modified spark plugs and therefore are unable to resolve spatial distribution. Other high-speed optical EGR measurements have been made using non-dispersive infrared (NDIR) sensors coupled with long capillaries to sample the intake gas[23,24] for ex situ diagnostics. Simultaneous measurement of temperature at the capillary tip has also been demonstrated.[25] Exhaust gas recirculation measurements in the intake manifold have also been demonstrated by probing the same CO_2 absorption band near 4.3 μm[26] or a H_2O absorption feature near 1.38 μm[27] using a tunable diode laser absorption spectroscopy (TDLAS). Both NDIR and TDLAS can provide similar results but require much higher initial investment than the proposed sensor.

This paper describes a fast, in situ diagnostic technique for measuring transient CO_2 concentration distributions in the intake manifold of a multi-cylinder IC engine. A direct absorption spectroscopy (DAS) technique was employed in conjunction with affordable MIR light-emitting diodes (LEDs) and a suitably minimally invasive measurement probe to provide a cost-effective EGR diagnostic technique that can give quick feedback during engine development. Two LEDs, modulated at different high frequencies, selectively probe two distinct regions in the MIR spectrum to deduce CO_2 concentrations in the intake manifold. The measurement probe provides for spatial resolution and other benefits to practical engine studies. Optical components and the sensor probe were carefully optimized for signal-to-noise ratio (SNR) and high measurement accuracy in the challenging on-engine conditions and require minimal modifications to the evaluated hardware. The sensor provides ±0.1% accuracy at 3% (cm^3/cm^3) CO_2 in a well-controlled intake manifold environment and resolves cylinder-specific engine stability at a rate of up to 1 kHz. References to CO_2 concentration throughout are in percent volume ratio (cm^3/cm^3), and the units are not typically specifically indicated.

SPECTROSCOPY

Electromagnetic radiation absorption occurs when the energy of a resonant photon is transferred to a molecule through light-matter interaction. Absorption is a very selective process and is highly dependent on molecular structure. In the MIR spectrum, rotational–vibrational (rovibrational) transitions of many combustion-related species can be probed to better understand the overall combustion process. Figure 1 shows the MIR rovibrational bands of the major combustion-product species CO_2 and H_2O and how H_2O is a major interference species of CO_2 in this spectral range and must be accounted for when developing a diagnostic technique. Carbon dioxide has three distinct absorption bands in the MIR spectrum: near 2.0, 2.7, and 4.3 μm. Each band is made up of many individual absorption features that correspond to different rovibrational transitions. Of the three absorption bands, the two CO_2 combination bands near 2.0 and 2.7 μm significantly overlap with water absorption features and are thus vulnerable to H_2O interference. Moreover, because LEDs have broad spectral emission profiles several orders of magnitude greater than the linewidth of an individual absorption feature, they lack the spectral selectivity required for accurate and interference-free assessment of CO_2 concentration when overlapping or adjacent interference features are present. The absorption band near 4.3 μm (fundamental ν_3), on the other hand, is entirely free of H_2O interferences and therefore provides a basis for spectroscopic quantification of CO_2 in an engine exhaust stream using spectrally broad LED sources. In addition, this band has the strongest absorption cross section, which is usually desirable since it leads to a more sensitive diagnostics technique. In this case, however, measurements are limited to relatively short path lengths and small CO_2 concentrations since the extremely strong absorption can quickly lead to saturation and result in lower sensitivity.

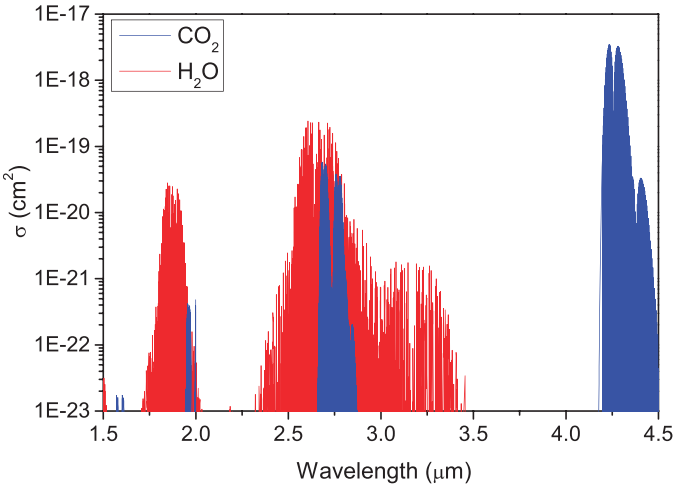

FIG. 1. Absorption cross section of CO_2 and H_2O in the MIR spectrum, 1 bar, 296 K; from HITRAN database.[28]

The diagnostic is based on spectrally integrated broadband absorbance, which offers some insensitivity to pressure and temperature fluctuations. Although the approach is not monochromatic or spectrally resolved on the scale of even individual absorption transitions, a stepwise approach most clearly conveys the diagnostic's

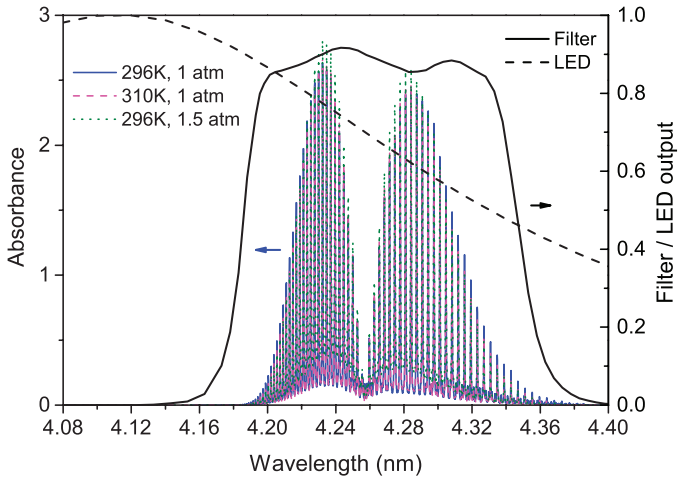

FIG. 2. Detailed absorbance spectra near 4.3 μm for 1% CO_2 and 14 mm path length at various temperatures and pressures. Spectrally resolved LED output and bandpass filter transmission curve is also shown.

theoretical basis. Absorption of monochromatic light is described by Beer–Lambert relations

$$\ln\left(\frac{I_T}{I_0}\right) = -\alpha = -\eta\sigma l \qquad (1)$$

where α is the absorbance (unitless), I_T is the transmitted signal light intensity (W/m^2), I_0 is the incident or reference light intensity (W/m^2), η and σ are number density (cm^{-3}) and absorption cross section (cm^2) of the target species, respectively, and l is the overall absorption path length (cm). Absorption cross section describes the likelihood of the gas absorbing a photon of certain wavelength and is temperature dependent primarily via the Boltzmann distribution. Although σ is unaffected by pressure under nominal conditions, its spectral shape (line shape) can broaden with increasing pressure; in conditions of low-to-moderate pressure fluctuations, σ can be considered pressure independent. A detailed list of all these parameters of σ can be found in the HITRAN database.[28] The Beer–Lambert equation strictly applies only if the light source is monochromatic, or at least much more spectrally narrow than the absorption feature.

Broadband linear regime absorption can be considered an infinite ensemble of monochromatic absorption units, and its theory is practically addressed via modifying the absorbance to include a spectral line shape function ϕ_ν (unitless); i.e., the absorbance becomes $-\eta\ \sigma\ l\ \phi_\nu$. Figure 2 shows the theoretical spectrally distributed CO_2 absorbance in the range applicable to the diagnostic and based on the HITRAN database. The spectra includes 1684 lines above a threshold of $S = 10^{-24}$cm^{-1}/(molecule $\times$ cm^{-2}), where S is line intensity specified in HITRAN.[28] The simulated spectra was calculated between 4.184 and 4.386 μm, a small region of the MIR spectra encompassed by the diagnostic's combined LED and bandpass filter spectra. The spectral emission used for broadband absorption is the product of the LED and filter functions shown in Fig. 2 and is relatively flat and featureless across the entire absorption CO_2 band. In addition to broadband excitation, the diagnostic uses broadband detection that does not spectrally resolve variation on the scale of the individual absorption lines. This is equivalent to spectrally integrating the product of the absorbance, filter, and LED curves shown in Fig. 2, which further demonstrates how the diagnostic is relatively insensitive to certain temperature and pressure variations. Pressure variations will change the absorption linewidths, and temperature variation will change the absorption cross-section distribution as described by the Boltzmann distribution. However, such temperature- and pressure-induced spectral redistributions of the absorbance are very small relative to the spectrally coarse scale of the LED-filter product spectral distribution and will generally be significantly dampened in the broad spectral integration. This is demonstrated in Fig. 2, where the theoretical absorbance is shown for three reference conditions spanning those typical of the diagnostic's intended application; specifically, the associated spectral absorbance variations with temperature and pressure are practically imperceptible on the scale of the LED and filter functions and will result in measurement variation of 0.1 and 2.5% for pressure and temperature, respectively, based on the broad spectral integration used, i.e., from 4.12 to 4.40 nm in Fig. 2. Concentration variations change the absorbance magnitude, which is not lost in the spectrally broad integration. Thus, the broadband diagnostic provides for measurements specifically sensitive to concentration and generally insensitive to temperature and pressure fluctuations.

The broadband diagnostic is not confined to the linear-absorption regime, and such mixed-regime broadband absorbance is described by curves of growth. Curves-of-growth theory is traditionally applicable to stellar spectroscopic analysis, where the spectral resolution is not sufficient to resolve individual absorption transitions, and the recorded spectrum is a composite of mixed-regime (i.e., linear and nonlinear) absorbance; in such cases, curves of growth are used to estimate line shape parameters, e.g., full width at half maximum (FWHM). In optically thin conditions, all 1684 CO_2 absorption transitions shown in Fig. 2 are in the linear-absorption regime, and the absorbance will increase linearly with concentration; of course, there are many more transitions below the specified threshold value that are not considered in this discussion. At some CO_2 absorption, the transitions with higher absorption cross sections will begin to saturate while the weaker transitions will remain in the linear-absorption regime. Such transition to saturation creates nonlinear absorption, wherein absorption signal no longer changes linearly with concentration changes. The result is that the broadband spectrally integrated diagnostic may have non-linear response at higher concentrations, as will be seen. However, since the diagnostic is based on broad band spectrally integrated measurements and does not seek to resolve individual line shape parameters (and is by design uniquely insensitive to variations in the line shape parameters), curves of growth are not directly relevant to the diagnostic theory but are mentioned because of their general relevance to broadband spectroscopy.

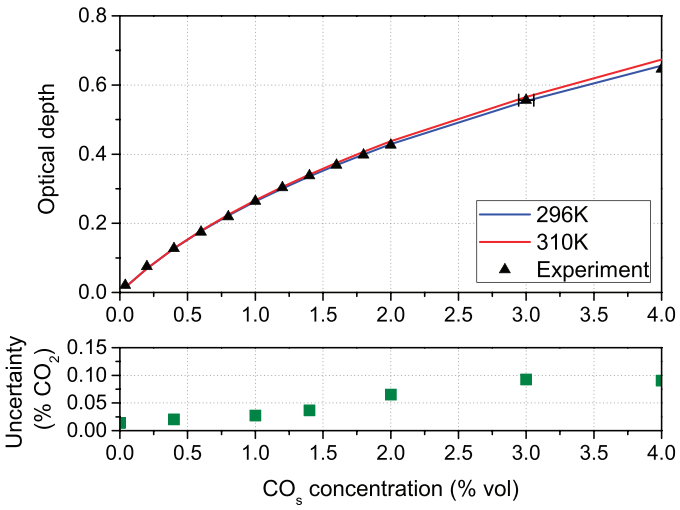

FIG. 3. Experimentally measured and calculated calibration curves. Calibration was performed at 296 K and 1 atm, and the calculations were performed at 296 and 310 K. Experimental data agree extremely well with theoretical results at 296 K. The calculated calibration curves show acceptable variations of 2.5% at the highest measured CO_2, but agree very well at lower concentrations. CO_2 measurement uncertainty due to the residual is also shown.

The diagnostic was calibrated to quantify its response and precision. For calibration, the EGR probe (described in Experimental Setup) was inserted into a flowing gas cell where a range of CO_2 concentrations were spanned using CO_2 standards balanced with N_2 and in a temperature- and humidity-controlled laboratory environment. Although engine applications are expected to introduce vibrations not present during calibration, these are not expected to affect the measurement because vibrations do not change the CO_2 spectroscopy; indeed, there was no noticeable change in the ambient CO_2 measurement in engine applications when operating with different levels of vibration, e.g., engine off versus motoring versus running with zero EGR or operating with zero EGR at different speed-load conditions.

Figure 3 shows a comparison of the measured and calculated calibration curves. The temperature and pressure of the calibration cell was held constant at 296 K and 1 atm, respectively, and the light source was stable throughout the experiment. The measured data shows the expected transition from the linear- to nonlinear-absorption regime as discussed earlier. The calculated calibration curves were determined as described earlier; specifically, each point on the calculated curves corresponds to the spectrally integrated product of the absorbance, LED, and filter functions in Fig. 2 at the CO_2 concentration, temperature, and pressure specific to that point. Simulated results at 296 K show good agreement with measured data; any difference between these 296 K data sets simply indicates a practical experimental factor not accounted for in the theoretical analysis, e.g., some small error in the LED or filter profiles, additional broadband losses in the optical train. The agreement of the 296 K data sets demonstrates the validity of the theoretical spectroscopic basis of the diagnostic described earlier. A simulated curve is also shown at 310 K, the intake-manifold temperature during engine applications, and can be used to quantify the diagnostic temperature sensitivity. Differences between the two simulated curves are relatively small, excellent agreement at the lower concentrations and a maximum difference of 2.5% at the highest measured CO_2 concentration. Because this maximum temperature sensitivity is small relative to engine operation variations, it was used as a general bound, and further consideration of the lower sensitivities throughout the applicable EGR range were not considered. The results in Fig. 3 demonstrate how the diagnostic is uniquely sensitive to concentration changes and uniquely insensitive to temperature (and pressure) changes, as discussed earlier. In engine applications, the experimentally verified 296 K theoretical calibration curve was used to convert measured signal into CO_2 mole fractions on a near-real-time basis. Despite slight difference in calibration and experiment temperatures, the diagnostics technique achieved $\pm 0.1\%$ (cm^3/cm^3) CO_2 measurement accuracy at 3% CO_2, i.e., 3.3% relative accuracy. Such resolution roughly equates to differentiating a 1% point change at 25% EGR fraction in an engine, which was the primary specification associated with the probe's development. This analysis and approach only applies to a specific engine configuration and near-ambient operating conditions considered for this paper. For applications in more extreme environments, such as in the exhaust where significant temperature and pressure fluctuations are expected, additional analysis and possibly parallel measurements of temperature or pressure may be required for a more complex calibration.

The intended engine applications involved near-ambient conditions, possibly with small temperature and pressure fluctuations no greater than those indicated in Fig. 2. Intake manifold temperature and pressure were expected to be stable and near 310 K and 1 atm, respectively, during steady operation with cooled EGR. Thermocouple-based low-speed intake-manifold temperature measurements were constant during steady operating conditions, but 2% temperature fluctuations were expected based on 1D fluid flow simulations (GT-Power). High-speed pressure transducer measurements indicated 3% pressure fluctuations inside the manifold during steady operation. These temperature and pressure fluctuations were likely due to oscillatory nature of EGR in the intake. However, as discussed earlier, they do not significantly affect the CO_2 concentration measurements.

EXPERIMENTAL SETUP

Exhaust Gas Recirculation Sensor. A schematic of the EGR sensor and probe is shown in Fig. 4. The LED assembly (LEDs and beam splitter) and detector are situated remotely in a controlled environment away from the engine and connected to the probe via two flexible light guides. The sensor is based on signal and reference beams from two LEDs with different center wavelengths. The signal LED overlaps with the CO_2 absorption band, and the reference LED overlaps with no known absorption bands of major combustion-product species. The signal LED, centered at 4.15 μm (Ioffe, LED42Sr via Boston Electronic Corp.), measures CO_2 absorption and non-absorption losses such as scattering and attenuation, e.g., from soot-fouled optics. The

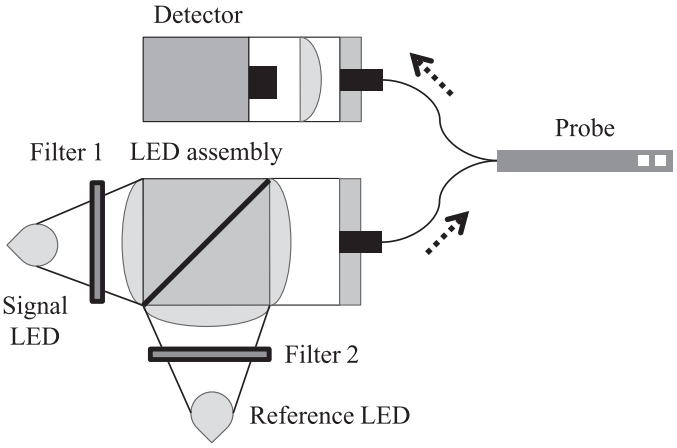

FIG. 4. Schematic of EGR sensor and probe. For a detailed probe dimension see Fig. 5. HWG NA is 0.05. LEDs and optical components in both the LED and detector assembly were optimized for maximum light coupling with the two HWGs.

reference LED, centered at 3.8 μm (Ioffe, LED38Sr via Boston Electronic Corp.), measures only non-absorption losses. The LED emissions have similar broadband profiles, FWHM 0.45 μm, far-field pattern FWHM $\leq 20^{\circ}$ despite differences in center wavelength.[29] Bandpass filters (4.26 μm λ_c with 0.15 μm FWHM for the signal LED, and 3.6 μm λ_c with 0.14 μm FWHM for the reference LED; filters via Andover Corp.) were added to restrict spectral emissions of both signal and reference LEDs. Light-emitting diodes were modulated at different high frequencies (50 and 77 kHz) to eliminate crosstalk between the two beams and reject interferences from the engine, such as vibration and gray body radiation. Light from the two LEDs was collimated using dedicated short-focal-length optics ($f = 50$ mm) and combined using a Pellicle beam splitter.

The combined signal and reference beams were coupled into a 1000 μm ID core pitch hollow wave guide (HWG; NA = 0.05, Polymicro Technologies) and guided to the probe tip, the only section of the sensor exposed to the flow field of interest. Hollow wave guides are flexible fused-silica capillaries with reflective internal silver halide coatings. They have relatively small bending losses and transmit an extremely wide range of MIR spectrum. The transmitted beams are recoupled into a 1000 μm ID core catch HWG and guide to a MIR detector sampling at 1 MHz to satisfy the Nyquist criterion. The complex detector signal was divided into 1000 consecutive data point samples, and each sample is individually Fourier transformed. The selected sample size is an ideal balance between temporal resolution and measurement accuracy, since sample size is inversely proportional to the former and proportional to the latter by affecting the frequency resolution and amplitude of discrete Fourier transform. Transformed amplitudes at the signal and reference LEDs' modulation frequencies were extracted to isolate interferences from soot and other scattering particles. The ratio of the two amplitudes was used to infer absorption intensity. For the given hardware configuration, the maximum temporal resolution was limited to 1 kHz due to the data acquisition system band width of 1 MHz and memory size of 1 M samples.

Exhaust Gas Recirculation Probe. The EGR probe is an integral part of the sensor because it provides the probing volume in the flow of interest and enables spatially resolved measurement. The compact 3/8 inch (9.525 mm) outer diameter probe houses optical elements and mechanical parts required to secure the elements in place during engine operations. Figure 5 shows a schematic and pictures of the probe assembly. Two rectangular openings near the probe tip are entrances to the probe's measurement ducts (i.e., measurement or probing volume), through which the measurement gas flows and interacts with the signal and reference LED light. A window separates the HWGs from the measurement region and gas mixture to be measured. Two spacer assemblies secure a mirror and lens, and the lens separates the two probe measurement ducts. The lens (effective focal length = 2.88 mm) allows longer absorption path length (better sensitivity) and improves the coupling efficiency between the pitch and catch HWGs, without which the transmitted signal would not be able to overcome substantial transmission loss of the catch HWG (1.5 dB/m). The sample gas flows through the probe measurement ducts perpendicular to the beam path (into the page in Fig. 5) on either side of the lens as denoted by gray arrows in the figure. The effective absorption path length is 1.4 cm round trip. The entire optic-spacer assembly along with the pitch and catch HWGs are secured by a fastener and clamp on the opposite end of the probe body. Since absorption is a path-integrated measurement, the EGR probe provides a measurement of CO_2 concentration averaged over the spatial extent of the probe measurement ducts, i.e., ~8 mm.

The length of the probing volume dictates the spatial resolution of the probe. Spatial EGR variations can be resolved by translating the probe volume into and out of the intake manifold even though the base measurement technique has no inherent spatial resolution within the absorption path length. In such a fashion, the EGR probe can resolve spatial EGR gradients across the entire flow field of interest. The overall length of the probe can be adjusted to cover the range of interest for a given application. For the purpose of this paper, the overall probe length was 25 cm. The probe was secured to the measurement region (e.g., intake manifold) using a bore-through NPT-compression (Swagelok, SS-600-1-4BT) fitting and a non-swaging graphite ferrule (SGE International 072615) to allow probe tip mobility; such access is suitably minimally invasive, requiring little to no modification to existing engine hardware (Fig. 6). Despite the probe's minimally invasive nature, it is a physical probe, and some flow disturbance is unavoidable, and the degree of disturbance may vary with the sensor tip position in the manifold and the specific engine-hardware geometry being investigated; indeed, for certain specific applications, computational fluid dynamics (CFD) analysis has shown probe-induced wake effects for several downstream diameters. However, CFD analysis has also shown minimal flow disturbance is introduced at the probe volume where the measurement is being made, allowing the gases to flow through

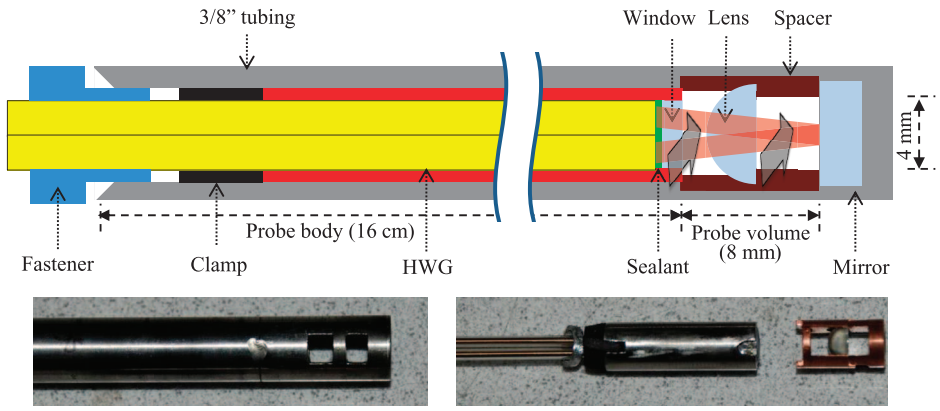

FIG. 5. Cross section of the EGR probe. Shown with optical and mechanical components. Overall measurement path length is 14 mm. Gray arrows indicate charge gas flow direction. The lower pictures show the probe and internal optical and mechanical components.

with very little restrictions. This enables the probe, despite its larger overall dimension, to achieve such a small spatial resolution. In addition, long-term measurements showed that the presence of the probe had no effect on the overall engine stability. For these reasons, the spatial resolution is defined as the distance over which the absorption measurements are made, i.e., 8 mm, or the distance between the window and mirror in Fig. 5. Potential additional application-specific flow effects from the probe should be considered when interpreting the measurements. Nevertheless, as shown in the following application sections, the EGR probe provides valuable information regarding the spatiotemporal uniformity of EGR-air mixtures in operating engines.

Another major benefit of the compact EGR probe is that it broadens applications and hastens advanced engine-system development by reducing the required optical access points from two down to one. In traditional line-of-sight diagnostics, light sources and detectors are positioned on opposite sides of the flow of interest. In fact, the initial EGR-sensor validation was performed using this classic configuration by mounting the detector directly onto an exhaust manifold and launching the LED-assembly light from the opposite side via an HWG. Such a setup, although maximizing signal sensitivity due to longer path length, is more susceptible to vibrational interference and, in many cases, is not feasible due to space constraint in and around a well-packaged engine. The compact form factor or the probe and flexible light guides allow quick assessment of EGR distribution at multiple intake manifold locations. The probe is also designed to be easily disassembled, cleaned, and reassembled to minimize engine down time. A simple pipe cleaner dipped in solvent was enough to thoroughly clean the probe. Under normal operation, one or two cleanings per day was sufficient to maintain the intended probe performance.

Engine. Development and demonstration of the EGR sensor for on-engine spatiotemporal EGR measurements was performed using an engine-dynamometer research facility in the Fuels, Engines, and Emissions Research Center at Oak Ridge National Laboratory. The engine was a four-cylinder General Motors (GM) 1.9 L diesel engine equipped with a high-pressure common-rail fuel-injection system, variable-geometry turbocharger, and a cooled high-pressure EGR loop. The engine control system calculated external EGR fraction by taking the ratio of mass flow rates in the intake and EGR loop. The cylinder firing order was 1-3-4-2 and driven by a fixed exhaust cam that maintains constant intake- and exhaust-valve timing regardless of engine speed. The specifications for the engine are presented in Table I.

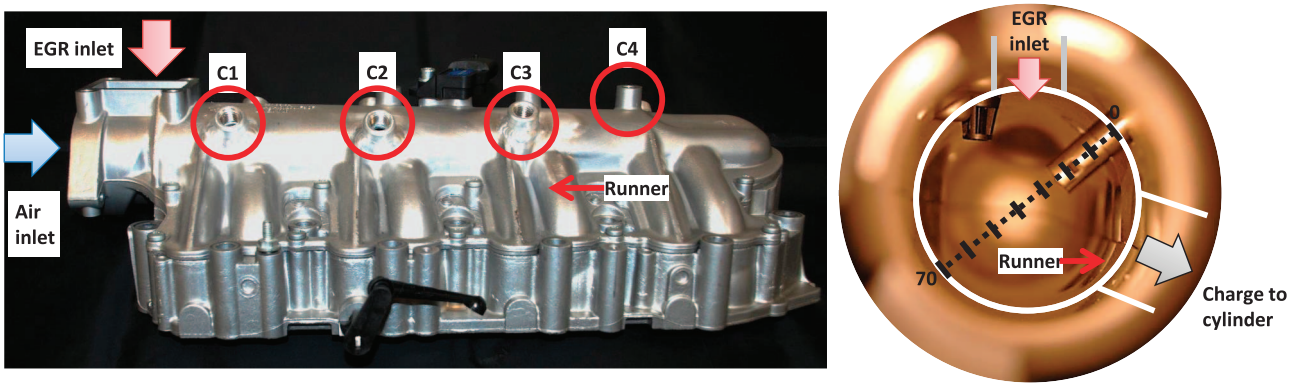

FIG. 6. (**left**) Picture of the intake manifold with minimal modification for EGR probe access. Axial measurement locations above the four cylinder-runner pairs are shown (C1–C4) as well as the air and EGR valve/inlet location. (**right**) EGR probe positioned inside the main intake plenum viewed through the air inlet, and with the intake runners taking off at the lower right. Radial probe location is also overlaid (0–70 mm).

The engine was managed using a National Instruments Labview-based control unit developed by Drivven Inc. The Drivven system allows for full control over the various engine parameters and was used to vary the fueling rate to each cylinder as well as EGR valve control. Figure 6 shows the intake manifold, which has two runners per cylinder and a variable-swirl actuator; cooled-EGR (~310 K) was metered by a stock valve and entered normal to the intake-air flow and just upstream of the cylinder 1 (C1 in Fig. 6) intake runners. The engine operator could set a specific EGR fraction, program EGR-valve modulations, or allow the control software to automatically adjust the settings in accordance with the original engine map supplied by the manufacturer. Bosses (6.35 mm NPT) were added to the intake manifold for EGR-probe access at axial measurement locations (C1–C3 in Fig. 6) above each intake runner pair leading to their corresponding cylinders; the C4 boss was offset due to hardware interference. Due to the orientation of the intake manifold on the engine, line-of-sight measurements were not practical, thus demonstrating the need for a single-point optical-access diagnostic technique. The probe was designed to traverse the entire internal diameter of the intake manifold, or 70 mm, at roughly 45° from the horizontal (Fig. 6). The compact probe allowed the major features of the intake manifold relevant to EGR spatiotemporal uniformity to occur as intended with minimal interference. Radial measurements were made continuously along the probe path (shown by the blue dotted line in Fig. 6). Length markers on the probe were used to determine the radial location of the probe volume. The presence of the probe at any measurement location had little to no effect on downstream cylinder operations as well as overall engine performance.

RESULTS AND DISCUSSIONS

The EGR probe performance for resolving spatial and temporal EGR uniformity was demonstrated via in situ engine measurements. Spatially resolved EGR measurements were made at the C1–C3 locations (Fig. 6) downstream from the EGR valve. At each axial location, radial-distribution measurements were made along the probe path across the main intake-manifold plenum in 10 mm increments from 5 to 65 mm (Fig. 6). Experiments were performed at various engine speeds and EGR fractions. Temporally resolved EGR measurements were made at the C1, 5 mm location, with the engine operating at various speeds and cylinder-to-cylinder fueling rates. The EGR probe was able to resolve significant spatial and temporal EGR variations via these intake-manifold measurements as discussed individually below.

Spatially Resolved Measurements. Non-uniform EGR distribution can cause cylinder-to-cylinder charge variations, inducing unbalanced performance between cylinders in a multi-cylinder engine. This leads to larger engineering margins (i.e., less optimized performance to accommodate such variations), which limits overall efficiency. Particularly for engine systems using high-pressure EGR, charge gas non-uniformity can limit efficiency if different cylinders take in different EGR fractions. This can cause cylinders closer to the EGR valve, with less residence time for the EGR-air charge to fully mix, to receive excessive or insufficient EGR charge, and lead to those cylinders behaving differently (cylinder-to-cylinder variations). Spatially resolved measurements were performed at 1000 and 1800 rpm, 50 ft·lb (67.8 N·m) torque. Two different EGR fractions were investigated at each engine speed; the specific EGR values differed slightly for the two speeds because the engine-control software was set to provide the most stable engine operation at each speed. Steady state CO_2 concentrations, measured using an independent FT-IR, for the low- and high-EGR conditions at 1000 rpm were 1.4 and 3.4%, respectively; the corresponding values at low- and high-EGR conditions at 1800 rpm were 1 and 2.8%, respectively. Along with the NDIR, the FT-IR is an industry standard for measuring time-averaged intake and exhaust species concentrations. A dedicated emission bench was not available or the engine exhaust, and therefore separate (FT-IR or NDIR) CO_2-based EGR fraction measurements were not obtained. Therefore, all subsequent comparisons between the probe and FT-IR are made based on CO_2 concentrations. Spatially resolved EGR distribution measurements were cycle averaged and thus do not show local high-speed EGR transients, which are discussed in the next section. At each spatial location, the measurements were sampled at a rate of 500 Hz and time-averaged over 167 and 300 engine cycles at 1000 and 1800 rpm, respectively.

TABLE I. Specifications of the multi-cylinder engine used for EGR diagnostic development.

Number of cylinders	4
Bore (mm)	82.0
Stroke (mm)	90.4
Compression ratio	17.5
Rated power (kW)	110 at 4000 rpm
Rated torque (Nm)	315 at 2000 rpm

The resulting EGR spatial distribution (Fig. 7) revealed significant intake-manifold charge-gas non-uniformity under certain engine conditions and locations and were expected to induce cylinder-to-cylinder performance variations. Specifically, notably higher CO_2 concentrations were measured along the near wall (5 and 15 mm radial locations) at the C1 access port closest to the EGR valve; these were most obvious at the high-EGR condition, but existed to some extent at all engine conditions studied. Because this near-wall region is closest to where the cylinder runners breathe from the main intake plenum (Fig. 6), it is likely that the C1 cylinder breathed a more concentrated EGR charge. Even with the existence of these regions of locally higher EGR fraction at the near-wall region of the C1 location, the corresponding center and far-wall-region EGR fractions were generally close to the value commanded via the engine-control software and in agreement with independent FT-IR measurements sampled from the intake manifold between the C2 and C3 locations. The highest CO_2 concentration peak occurred at the slower engine speed and higher EGR fraction; notably, the engine was prone to misfire at this same condition,

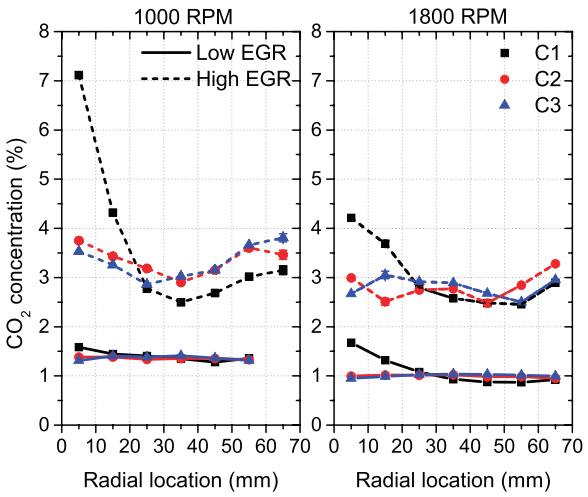

FIG. 7. Cycle-average spatial distribution of exhaust gas in the intake manifold. The low- and high-CO_2 concentrations as measured by an FT-IR were 1.4 and 3.4% at 1000 rpm, and 1 and 2.8% at 1800 rpm. Error bars are indeed shown for each point but are smaller than the point markers.

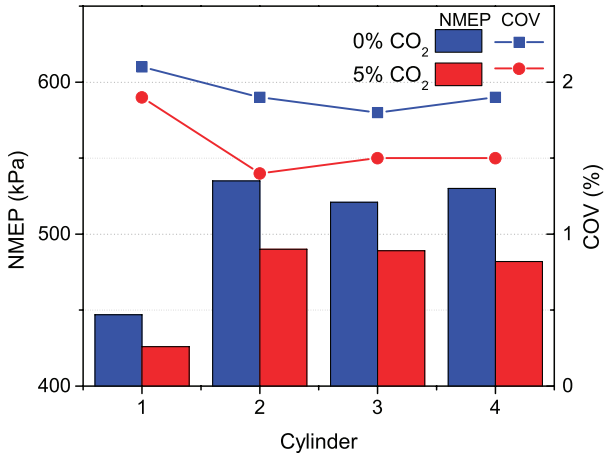

FIG. 8. Cylinder-specific NMEP and COV of NMEP at 0 and 5% CO_2 in the intake manifold at 1000 rpm. Cylinder 1 exhibits substantially lower NMEP and higher COV than other cylinders due to exhaust-gas maldistribution.

possibly in part due to a greater C1-cylinder EGR fraction induced by the non-uniform EGR as discussed above.

The exhaust-gas distribution became more homogeneous at the downstream (C2 and C3) locations, especially at the low-EGR condition. Based on the unique non-uniform C1 EGR distribution and the similarly uniform C2 and C3 distributions, it is apparent that practical EGR-charge uniformity was achieved between the C1 and C2 locations. This suggests that significant improvements to the cylinder-to-cylinder charge uniformity could be achieved by correspondingly increasing the mixing length between the EGR inlet and C1 locations; more detailed understanding of the required mixing length could be provided by additional measurements between the C1 and C2 locations. However, simply increasing mixing length may not be a practical solution due to engine-packaging limitations.

At higher EGR fractions, greater spatial variations were observed at all speeds and locations. However, unlike the variations at the low-EGR conditions, the near-wall CO_2 concentration variations at C1 were smaller at the higher engine speed. Pockets of low EGR were observed near the center of the intake manifold and throughout the C1-to-C3 length at the 1000 rpm, high-EGR condition. These variations were greater than the measurement uncertainty. These low-EGR pockets may be due to higher exhaust-to-intake pressure differential causing the exhaust gas to jet out of the EGR valve and hug the intake-plenum walls, rather than mixing into the flow core as occurred at the higher speed; although the higher engine speed produced higher exhaust-manifold pressure, it also created greater turbocharger boost, which led to the possibly counterintuitive lower pressure differential. The significantly greater EGR charge at the C1 near-wall location may have caused the first cylinder to breathe a greater EGR charge compared to downstream cylinders. Inhomogeneous charge-gas distribution in a multi-cylinder engine can lead to reduced engine performance and efficiency as a result of calibration compromises needed to compensate for such cylinder-to-cylinder differences, which can be significant as shown in Fig. 8, where significant variations in cylinder-specific net mean effective pressure (NMEP) and coefficient of variation (COV) of NMEP can be observed between the first and the remaining cylinders.

The performance of two passive EGR mixer designs was assessed via spatially resolved intake CO_2 measurements on an engine at the Cummins Technical Center in Columbus, Indiana; these measurements were specifically intended to assess certain numerical design tools and assumptions, and the results do not reflect optimized or production EGR uniformity. Although the details of the specific engine conditions and mixer designs are not discussed here, this application is included to demonstrate actual use of the EGR probe for advancing engine technology and the associated development models. The intake hardware generally consisted of an intake throttle, EGR inlet and mixing section, and intake manifold (generally like a long plenum with runners for the various cylinders). The mixers were evaluated under high- and low-EGR conditions. The radial EGR uniformity across the intake plenum was measured at axial locations aligned with the first three cylinder runners, CC1–CC3, where CC1 corresponds to the first cylinder downstream of the EGR inlet and mixing section. Exhaust gas recirculation probe access was made using bosses like those shown in Fig. 6, but oriented to translate across the plenum and into the runner throat on the far side; translation was performed in 10 mm increments from 0 to 70 mm at CC1, and in 20 mm increments from 10 to 70 mm at CC2 and CC3. To determine the cycle-averaged spatial EGR uniformity, a new figure of merit was determined by calculating the COV of CO_2 concentration measurements along the probe path at each of the three measurement locations (CC1–CC3); COV is also known as the relative standard deviation and is the standard deviation of each data set (eight points for CC1, and four points for CC2 and CC3) expressed as a percentage normalized by the mean value of the corresponding data set. Figure 9 shows the measured spatial EGR uniformity expressed as COV, where lower COV indicates greater spatial

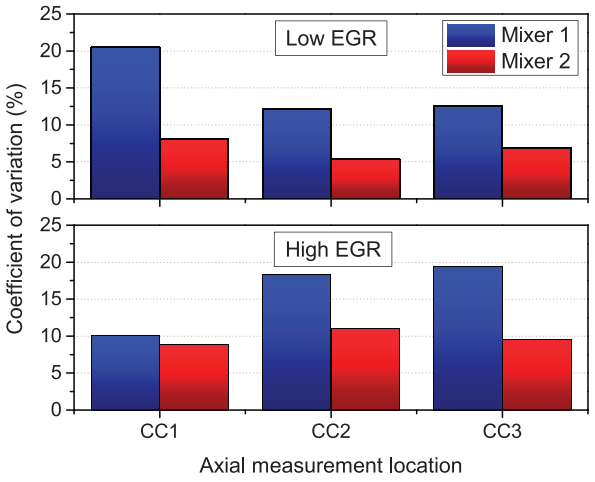

FIG. 9. CO_2 COV at various axial measurement locations. Two mixer designs were examined under low- and high-EGR conditions. Mixer 2 consistently produced more spatially uniform EGR for all conditions and locations.

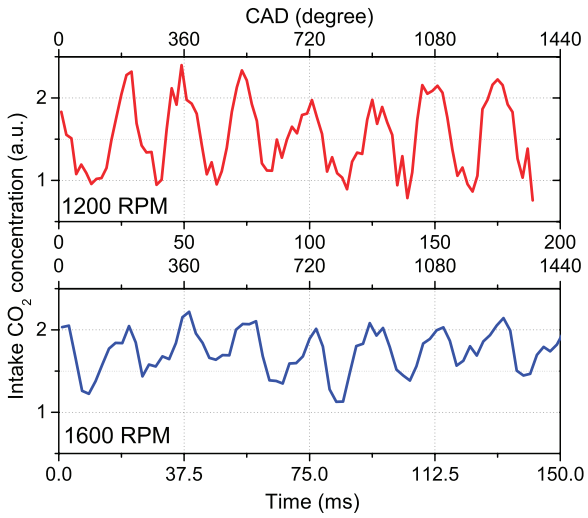

FIG. 10. Cylinder-timescale temporal response of the EGR probe. Cylinder-specific exhaust fluctuations of a four-cylinder engine at (top) 1200 rpm and (bottom) 1600 rpm.

uniformity, for the two mixer designs at the two different EGR fractions and the three intake-manifold locations. These results indicate that mixer 2 consistently produced a more spatially uniform EGR-air charge compared to mixer 1 at both low- and high-EGR fractions, by 54 and 34%, respectively, representing an average relative improvement of 44%. At lower EGR, the mixer differences were greatest near the EGR valve (CC1), whereas at high EGR, the differences were greatest further downstream (CC3). This delay is likely attributed to higher exhaust gas fractions requiring longer distance to fully mix. These and other more detailed spatiotemporally resolved results were used to assess specific modeling functions used for system design and promote development of improved efficiency mixers.

Understanding the spatial distribution of EGR is an important step in improving engine efficiency losses due to cylinder-to-cylinder EGR air-charge variations. The utility of the spatially resolving EGR probe is not limited to assessing EGR uniformity, but is applicable to other areas of efficient-engine development. With an appropriate light source, the probe could be adapted to accurately assess in situ species information in and around catalysts such as ammonia uniformity at the inlet to and within a selective catalytic reduction catalyst.

High-Speed Transient- Exhaust Gas Recirculation Measurements. In addition to spatial uniformity, temporal uniformity is desirable to achieve stable engine operation; instabilities will generally mandate greater engineering margins that reduce efficiency. For instance, intake-manifold resonances can create a moving EGR wave, which if synchronous with intake valve events could cause cycle-to-cycle and cylinder-to-cylinder combustion variations or instability. More likely are cycle-to-cycle variations caused by feedback inherent to the EGR hardware or loop; e.g., exhaust gas from a multi-cylinder engine subjected to cylinder-to-cylinder EGR variations will likely create a temporal train of irregular exhaust pulses, which when mixed with fresh air can cause cycle-to-cycle variation. To accurately monitor and reduce these unwanted small-timescale phenomena, the EGR probe must be fast enough to resolve cycle-timescale events. The origin of these temporal instabilities and their mitigation strategies can be further assessed with even faster cylinder and crank-angle temporal resolution measurements.

To assess the ability of the EGR probe to resolve cycle- and cylinder-timescale EGR transients, measurements were conducted using the engine system described in the Engine subsection, and with the probe at a fixed location (C1, 5 mm) where the exhaust-gas spatial variation was determined to be greatest. Data was acquired at a maximum temporal resolution of 1 kHz (7.2 and 9.6 crank-angle degrees (CAD) at 1200 and 1600 rpm, respectively). Although faster measurements may be required for higher rpm studies, 1 kHz was sufficient to resolve cycle-timescale EGR dynamics for engine speeds up to 2000 rpm; such faster measurements require the use of more powerful LEDs or a laser source, which we have since demonstrated.

To resolve small CO_2 fluctuations associated with exhaust-breathing (i.e., exhaust-valve) events, the bandpass filters in the LED assembly were removed to maximize output power and improve the SNR; although this may reduce the quantitative measurement sensitivity, it provides an opportunity to assess the ultimate temporal response of the EGR probe. The reconfigured sensor calibration was remapped to allow for limited quantitative comparison. Initial measurements were made at two different engine speeds, and the results at 1200 and 1600 rpm are shown in Fig. 10. In both cases, CO_2 fluctuations correlated well with engine timing; specifically, there are four EGR peaks per engine cycle, spaced according to cylinder-exhaust-valve timing, and independent of engine speed due to fixed exhaust-cam timing. This indicates that the specific exhaust-breathing events from each cylinder can be observed in the intake manifold (via the EGR loop), and cylinder-timescale fluctuations can be accurately measured by the EGR probe operating at 1 kHz. Such measurements are useful for designing mixers

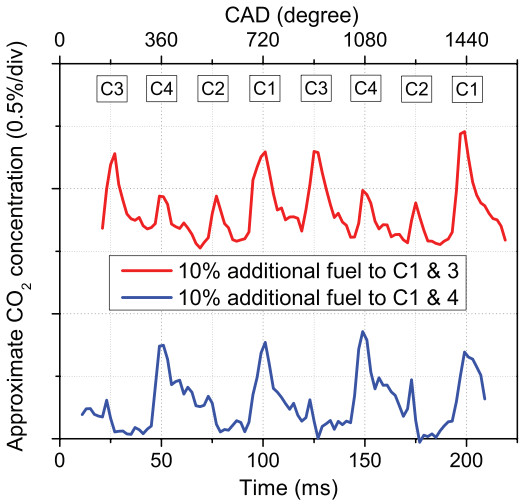

FIG. 11. Cylinder-specific CO_2 measurements using the EGR probe. 10% additional fuel was added to cylinders 1 and 3, and 1 and 4, producing correspondingly higher cylinder-specific CO_2 concentrations. Measured CO_2 peaks correspond well to engine timing and cylinder firing order. The boxed C-number legends indicate exhaust-valve timing of the corresponding cylinder.

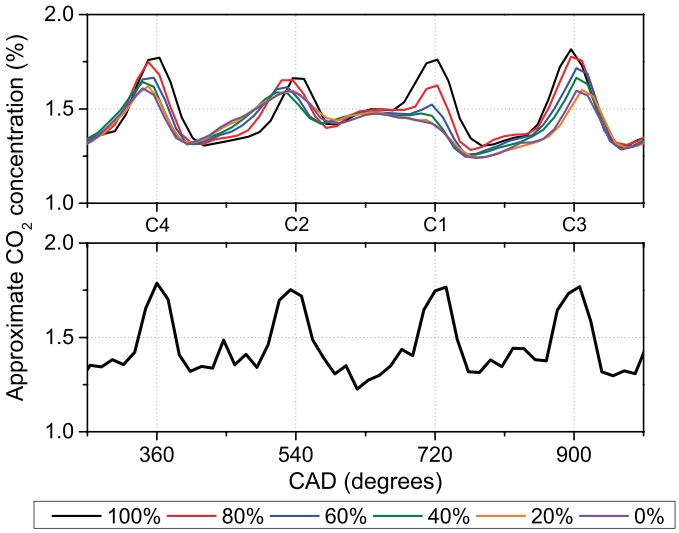

FIG. 12. Cylinder-specific CO_2 measurement across a single cycle at 1200 rpm with the EGR probe positioned at C1, 5 mm. (**top**) CO_2 dynamics associated with reduced fueling in cylinder 1 from 100 to 0% in 20% decrements. No combustion took place at 20 and 0% fueling. (**bottom**) Normal engine operation immediately after balancing the cylinders.

that homogenize the gas mixture both temporally and spatially.

To further demonstrate the ability of the EGR probe for resolving cylinder-specific combustion events, the cylinder-specific fueling was adjusted to induce cylinder-to-cylinder exhaust-CO_2 variations in the multi-cylinder engine. Specifically, 10% additional fuel was injected into two of the four cylinders, while operating at 1200 rpm, and with the base cylinder-to-cylinder fuel injection initially balanced; i.e., the base cylinder-specific fueling was tuned such that every cylinder produced the same levels of output based on indicated mean effective pressure (IMEP) calculated from in-cylinder pressure transducer data. Cylinder-to-cylinder IMEP variations were less than 1%. Overall, the engine produced 50 ft·lb (67.8 N·m) of torque. Figure 11 shows that the EGR probe was clearly able to detect the cylinder-specific exhaust-CO_2 dynamics associated with fueling changes to the specific cylinders. The cylinders with extra fueling produced consistently higher CO_2 concentrations than those with the base fueling. Moreover, the CO_2 dynamics were temporally aligned with the exhaust-valve timing as well as the firing order. In addition to resolving cylinder-specific exhaust-breathing events of the four-cylinder engine at 1600 rpm, each of which corresponds to about 19 ms, fast transients down to 4 ms were resolved with the probe operating at 1 kHz.

The same EGR probe and engine-system setup was used to demonstrate how this fast diagnostic with cylinder-resolved temporal resolution can be used to assess combustion completion figures of merit. Indicated mean effective pressure can be interpret as average in-cylinder pressure during an engine cycle such that a very stable engine would exhibit low COV of IMEP. For this demonstration, EGR probe measurements were made at the C1, 5 mm location while the cylinder 1 fueling was reduced from 100 to 0% in 20% decrements; this simulates various level of incomplete combustion, where 100 and 0% represents normal combustion and misfire, respectively. The cylinder-to-cylinder CO_2 peak amplitude differences at 100% fueling in the lower panel of Fig. 12 show CO_2 measurements from a recently balanced engine. The balanced results show similar levels of cylinder-to-cylinder CO_2 generation, indicating nearly uniform combustion across all cylinders.

The upper panel of Fig. 12 shows that the peak CO_2 corresponding to the cylinder 1 exhaust event progressively decreased as that cylinder's fueling was decreased from 100 to 40%, indicating a corresponding change in the cylinder 1 combustion. Independent in-cylinder pressure-transducer measurements of IMEP indicated similar changes. At 40% fueling, combustion phasing was extremely retarded, and combustion was barely detectable, as apparent from the practically negligible cylinder 1 CO_2 dynamic in Fig. 12. More interestingly, the CO_2 trace at 20 and 0% fueling indicated no combustion took place, as was confirmed via the separate in-cylinder pressure-transducer measurements. Exhaust events in the other cylinders were also affected by the cylinder 1 fueling; this may be due to changes in other engine parameters commanded or set by the engine control unit (ECU) in response to the manual cylinder 1 fueling override.

These experiments and those as outlined of Fig. 11 indicate that the EGR probe is capable of quantitatively assessing cylinder-to-cylinder and cycle-to-cycle combustion variations even in the intake manifold of a multi-cylinder engine where temperature and pressure fluctuations are relatively small. It may even be used to correlate the measured variations to combustion figures of merits, such as COV of IMEP. Understanding the high-speed EGR dynamics is crucial for developing EGR systems and intake manifolds that can distribute homo-

geneous charge gas to each cylinder in a multi-cylinder engine, thereby improving the overall engine efficiency.

CONCLUSION

A fast in situ EGR probe was developed based on absorption spectroscopy using MIR LEDs. The probe enables high spatial- and temporal-resolution single-access-port CO_2-concentration measurements with minimal flow disturbances and little to no modifications of the engine hardware. The compact probe design and flexible HWGs, which couple the light in and out of the probe tip, allows for remote sensing, thereby minimize the number and size of required optical-access points around the flow of interest. It is ideal for in situ analysis in well-packaged engines where space and access around flows of interest are limited. The probe can be translated to map a flow with 4×8 mm (corresponding to the overall dimensions of the probe's two measurement ducts) spatial resolution during engine operation. The sensor can be produced more cost effectively compared to laser-based sensors; however, it is still cost prohibitive as an onboard-diagnostics tool for the foreseeable future. Nevertheless, in its target application of engine-system development, the EGR probe provides broad insights relevant to advancing these technologies as highlighted herein. Being directly exposed to the intake EGR-air stream, the probe's optics are susceptible to deposits from particulate matter (PM), water, and hydrocarbon condensations. The analysis method using signal and reference LEDs mitigates the effect of PM deposits until these deposits occlude the signals to such a level that the SNR is unacceptable; however, for all the engine applications described herein, the probe was able to continuously operate for 4 to 8 h without cleaning. The probe has been designed and applied to the relatively uniform, low-temperature and atmospheric-pressure environment of an engine intake manifold, and the broadband nature of the LED-based spectroscopy mitigates the sensitivity of the measurement to variations in these parameters.

The durability and operability of the EGR probe was demonstrated via in situ measurements on full-scale engine systems. The probe was able to function in the presence of engine vibrations, soot, and other complex exhaust constituents; spatially resolve cycle-averaged non-uniformities of 0.1% CO_2 for CO_2 concentrations up to 4%; and temporally resolve cycle-timescale EGR fluctuations at speeds of up to 1 kHz. Spatial EGR distribution measurements were performed at various locations in the intake manifold and revealed significant spatial non-uniformities; a very concentrated unmixed exhaust stream existed along the main intake-plenum wall near the cylinder 1 runner inlets, and it is very likely that this caused the cylinder 1 EGR charge to be much greater than that of the other three cylinders. This technique was used to evaluate the performance of two passive mixers designed to improve EGR spatial uniformity and thereby reduce cylinder-to-cylinder variations. The results showed one mixer to be 44% more effective overall in homogenizing the charge gas and were further used to improve system-design modeling capabilities by providing spatially resolved measurements of EGR distribution that would otherwise be unavailable with conventional analyzers.

In addition, the probe was used to study high-speed EGR dynamics in the intake manifold induced by exhaust breathing events. Measurements made at 1200 and 1600 rpm temporally aligned with the cylinder exhaust-valve timing and firing order, indicating the ability to temporally resolve individual cylinder-exhaust events. Fast temporal resolution can provide information on short-timescale valve events and transient phenomena down to 4 ms that can be used to design more effective spatiotemporal mixers and ultimately improve engine performance and efficiency. The technique can therefore be used to promote faster technology development by enabling efficient evaluation of components and control schemes, improve mixing models and other numerical design tools, as well as demonstrate advanced closed-loop control strategies.

ACKNOWLEDGMENTS

This research was sponsored by the U.S. Department of Energy, Office of Energy Efficiency and Renewable Energy, Vehicle Technologies Office, with Gurpreet Singh, Ken Howden, and Leo Breton as the Program Managers, via a Cooperative Research and Development Agreement (CRADA) with Cummins Inc., Columbus, Indiana. The authors are also grateful to Eddie Raby and Michael Saale of Vacuum Technology Incorporated, Oak Ridge, Tennessee, for their efforts regarding timely manufacturing of the EGR probe necessary for meeting the project timeline and goals. Notice: This manuscript has been authored by UT-Battelle, LLC under Contract No. DE-AC05-00OR22725 with the U.S. Department of Energy. The United States Government retains and the publisher, by accepting the article for publication, acknowledges that the United States Government retains a non-exclusive, paid-up, irrevocable, world-wide license to publish or reproduce the published form of this manuscript, or allow others to do so, for United States Government purposes. The Department of Energy will provide public access to these results of federally sponsored research in accordance with the DOE Public Access Plan (http://energy.gov/downloads/doe-public-access-plan).

1. M. Zheng, G. Reader, J. Hawley. "Diesel Engine Exhaust Gas Recirculation–A Review on Advanced and Novel Concepts". Energy Convers. Manage. 2004. 45(6): 883-900.
2. C. Bowman. "Kinetics of Pollutant Formation and Destruction in Combustion". Prog. Energy Combust. Sci. 1975. 1(1): 33-45.
3. T. Murayama, M. Zheng, T. Chikahisa, Y. Oh, Y. Fujiwara, S. Tosaka, M. Yamashita, H. Yoshitake. "Simultaneous Reductions of Smoke and NO_x from a DI Diesel Engine with EGR and Dimethyl Carbonate". SAE Tech. Pap. Ser. 1995. 952518. doi:10.4271/952518.
4. D. Tomazic, A. Pfeifer. "Cooled EGR–A Must or an Option for 2002/04". SAE Tech. Pap. Ser. 2002. 2002-01-0962. doi:10.4271/2002-01-0962.
5. M. Zheng, G. Reader. "Preliminary Investigation of Cycle to Cycle Variations in a Nonair-Breathing Diesel Engine". J. Energy Resour. Technol. 1995. 117(1): 24-28.
6. M. Zheng, G. Reader. "An Experimental Analysis of EGR on Operational Stabilities of Diesel Engines". ASME Intern. Combust. Engine Div. Fall Tech. Conf., Proc. 1993. 36-1. 101-106.
7. M. Zheng, G. Reader, G. Galinsky, I. Potter, R.W. Gustafson. "Ignition Delay and Pressure-Time Characteristics in a Diesel Engine Using Carbon Dioxide and Argon Enriched Oxidants". Proc. Eng. Technol. Conf. Energy. 1993. 1-7.
8. J. Hansel. "Lean Automotive Engine Operation–Hydrocarbon Exhaust and Emissions and Combustion Characteristics". SAE Tech. Pap. Ser. 1971. 710164. doi:10.4271/710164.
9. L. Shi, Y. Cui, K. Deng, H. Peng, Y. Chen. "Study of Low Emission Homogeneous Charge Compression Ignition (HCCI) Engine Using Combined Internal and External Exhaust Gas Recirculation (EGR)". Energy. 2006. 31(14): 2665-2676.
10. J. Heywood. "Combustion in Spark-Ignition Engines". In: J. Heywood, editor. Internal Combustion Engine Fundamentals. New York: McGraw-Hill, 1988. Ch. 9, Pp. 371-490.

11. G. Abd-Alla. ‘‘Using Exhaust Gas Recirculation in Internal Combustion Engines: a Review’’. Energy Convers. Manage. 2002. 43(8): 1027-1042.
12. M.G. Allen. ‘‘Diode Laser Absorption Sensors for Gas-Dynamic and Combustion Flows’’. Meas. Sci. Technol. 1998. 9. 545-562.
13. E. Furlong, D. Baer, R. Hanson. ‘‘Combustion Control Using a Multiplexed Diode-Laser Sensor System’’. Proc. SPIE. 1996. 26(2): 2851-2858.
14. A. Farooq, J. Jeffries, R. Hanson. ‘‘Sensitive Detection of Temperature Behind Reflected Shock Waves Using Wavelength Modulation Spectroscopy of CO_2 Near 2.7 μm’’. Appl. Phys. B: Lasers Opt, 2009. 96(1): 161-173.
15. R.K. Hanson, P.K. Falcone. ‘‘Temperature Measurement Technique for High Temperature Gases Using a Tunable Diode Laser’’. Appl. Opt. 1978. 17(16): 2477-2480.
16. C. Bowman, R. Hanson. ‘‘Shock Tube Measurements of Rate Coefficients of Elementary Gas Reactions’’. J. Phys. Chem. 1979. 83(6): 757-763.
17. A. Farooq, J. Jeffries, R. Hanson. ‘‘CO_2 Concentration and Temperature Sensor for Combustion Gases using Diode-laser Absorption Near 2.7 μm’’. Appl. Phys. B: Lasers Opt, 2008. 90(3-4): 619-628.
18. P.A. Martin. ‘‘Near-Infrared Diode Laser Spectroscopy in Chemical Process and Environmental Air Monitoring’’. Chem. Soc. Rev. 2002. 31: 201-210.
19. M.S. Zahniser, D.D. Nelson, C.E. Kolb. ‘‘Tunable Infrared Laser Differential Absorption Spectroscopy (TILDAS) Sensors for Combustion Exhaust Pollutant Quantification’’. In: K. Kohse-Höinghaus, J.B. Jeffries, editors. Applied Combustion Diagnostics. New York: Taylor and Francis, 2002. Ch. 26, Pp. 645-664.
20. J.A. Silver. ‘‘Frequency-Modulation Spectroscopy for Trace Species Detection: Theory and Comparison Among Experimental Methods’’. Appl. Opt. 1992. 31(6): 707-717.
21. M. Hall, P. Zuzek. ‘‘Fiber Optic Sensor for Time-Resolved Measurements of Exhaust Gas Recirculation in Engines’’. SAE Tech. Pap. Ser. 2000. 2000-01-2865. doi:10.4271/2000-01-2865.
22. A. Grosch, H. Wackerbarth, O. Thiele, T. Berg, L. Beckmann. ‘‘Infrared Spectroscopic Concentration Measurements of Carbon Dioxide and Gaseous Water in Harsh Environments With a Fiber Optical Sensor by Using the HITEMP Database’’. J. Quant. Spectrosc. Radiat. Transfer. 2014. 133: 106-116.
23. C. Sutela, N. Collings, T. Hands. ‘‘Fast Response CO_2 Sensor for Automotive Exhaust Gas Analysis’’. SAE Tech. Pap. Ser. 1999. 1999-01-3477. doi:10.4271/1999-01-3477.
24. C. Sutela, N. Colings, T. Hands. ‘‘Real Time CO_2 Measurement to Determine Transient Intake Gas Composition Under EGR Conditions’’. SAE Tech. Pap. Ser. 2000. 2000-01-2953. doi:10.4271/2000-01-2953.
25. J.M. Luján, J. Galindo, J.R. Serrano, B. Pla. ‘‘A Methodology to Identify the Intake Charge Cylinder-to-Cylinder Distribution in Turbocharged Direct Injection Diesel Engines’’. Meas. Sci. Technol. 2008. 19(6): 065401.
26. R.M. Green. ‘‘Measuring the Cylinder-to-Cylinder EGR Distribution in the Intake of a Diesel Engine During Transient Operation’’. SAE Tech. Pap. Ser. 2000. 2000-01-2866. doi:10.4271/2000-01-2866.
27. G.S. Jatana, M. Magee, D. Fain, S.V. Naik, G.M. Shaver. , R.P. Lucht. ‘‘High-Speed Diode Laser Measurements of Temperature and Water Vapor Concentration in the Intake Manifold of a Diesel Engine’’. Int. J. Engine Res. 2014. 15(7): 773-788.
28. L. Rothman, I. Gordon, A. Barbe, D. Benner, P. Bernath, M. Birk, V. Boudon, L. Brown, A. Campargue, J.-P. Champion, K. Chance, L. Coudert, V. Dana, V. Devi, S. Fally, J.-M. Flaud, R. Gamache, A. Goldman, D. Jacquemart, I. Kleiner, N. Lacome, W. Lafferty, J.-Y. Mandin, S. Massie, S. Mikhailenko, C. Miller, N. Moazzen-Ahmadi, O. Naumenko, A. Nikitin, J. Orphal, V. Perevalov, A. Perrin, A. Predoi-Cross, C. Rinsland, M. Rotger, M. Simeckova, M. Smith, K. Sung, S. Tashkun, J. Tennyson, R. Toth, A. Vandaele, J. Vander Auwera. ‘‘The HITRAN 2008 Molecular Spectroscopic Database’’. J. Quant. Spectrosc. Radiat. Transfer. 2009. 110(9-10): 533-572.
29. B. E. Corporation. ‘‘IR LED product page’’. http://www.boselec.com/products/documents/IRLEDsWWW6-4-07.pdf [accessed Aug 7 2015].